A Direct Model Predictive Control Strategy of Back-to-Back Modular Multilevel Converters Using Arm Energy Estimation

Akseli Hakkila*, Antonios Antonopoulos†, Petros Karamanakos*
*Faculty of Information Technology and Communication Sciences, Tampere University,
33101 Tampere, Finland
Email: akseli.hakkila@ieee.org, p.karamanakos@ieee.org
†School of Electrical and Computer Engineering, National Technical University of Athens,
15780 Zografou, Greece
Email: antoniosantonopoulos@mail.ntua.gr

Keywords

≪Model Predictive Control≫, ≪Modular Multilevel Converters (MMC)≫, ≪Optimal control≫, ≪Multi-objective optimization≫.

Abstract

This paper presents a model predictive control (MPC) algorithm for modular multilevel converters (MMCs). To meet the control objectives of phase current reference tracking and circulating current minimization, the proposed control scheme calculates the optimal number of submodules (SMs) to be inserted in each arm. In doing so, favorable steady-state and dynamic performance is achieved. Moreover, by estimating—instead of measuring—the arm energies in the predictive stage of the control loop, the proposed control scheme results in self-stabilizing open-loop arm energy balancing, while avoiding potential stability issues. Furthermore, to reduce the computational complexity of the MPC algorithm, the optimization problem is simplified by controlling each phase separately and assuming that the SM capacitors are balanced within an arm. To ensure that this assumption is always satisfied, a subsequent capacitor voltage balancing algorithm is designed to select the individual SMs that are switched on and off. The performance of the proposed control strategy is validated with simulations for a high voltage dc system (HVDC) that consists of two MMCs with 20 SMs per arm in a back-to-back configuration.

Introduction

The modular multilevel converter (MMC) [1] is an excellent candidate for high-voltage applications, such as high voltage dc (HVDC) transmission systems [2], since its scalability allows operation at different voltage levels with low power losses and harmonic distortions. Control of MMCs, however, is a nontrivial task since multiple control objectives need to be simultaneously met. Specifically, output current reference tracking, circulating current elimination, and capacitor voltage balancing need to be achieved during both steady-state and transient operating conditions.

To achieve the above control goals, conventional control techniques are commonly employed that rely on linear control theory. Such methods decompose the multiple-input multiple-output (MIMO) control problem into several single-input single-output (SISO) control loops that are arranged in a cascaded manner and utilize proportional-integral (PI) controllers. Using cascaded control loops, however, works well in steady state, but it limits the transient performance since the system dynamics are not fully decoupled [3].

The aforementioned control issues, however, can be effectively tackled by modern control methods, such as model predictive control (MPC) [3]. MPC, especially in its version as direct controller (i.e., when a

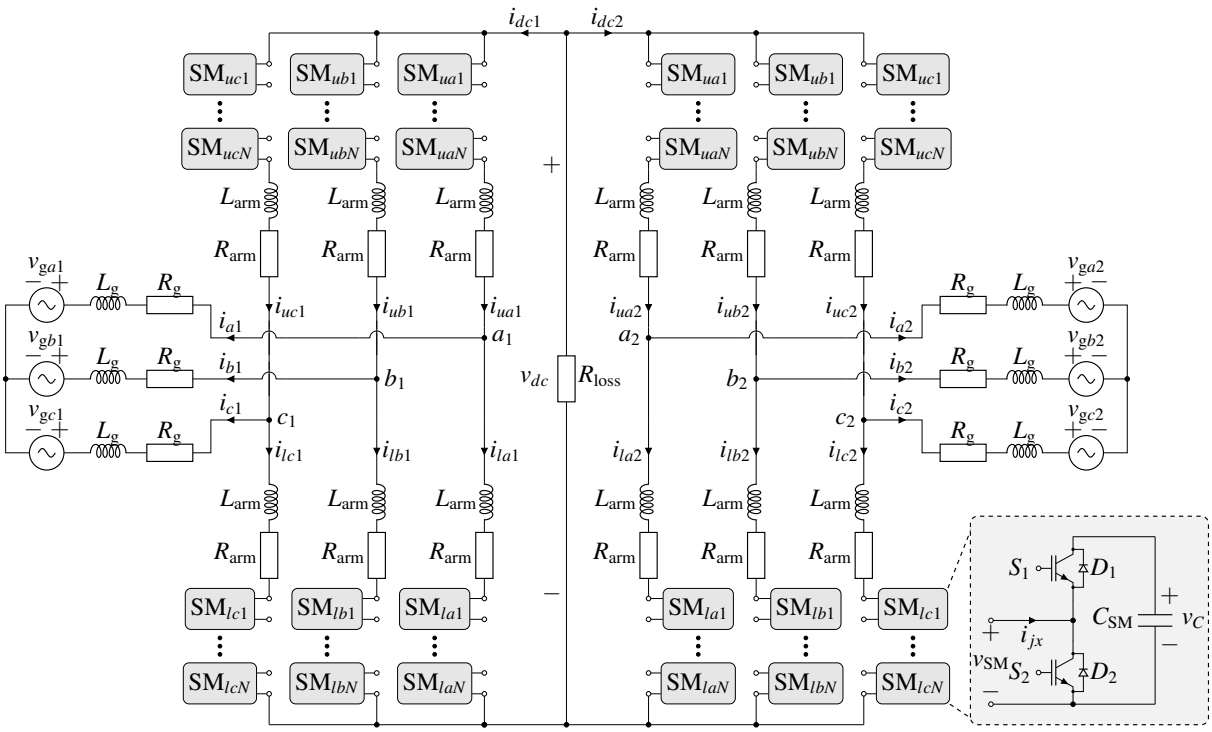

Fig. 1: Circuit diagram of a back-to-back connected MMC-HVDC system.

dedicated modulator is not used to generate the switching signals) can handle MIMO, nonlinear systems, such as MMCs, in a single control loop and address the multiple—and often conflicting—objectives in one computational stage [4]. Nevertheless, the lack of a modulator in direct MPC implies that the underlying optimization problem is an integer program (IP), which can be computationally intractable as its size increases [5]. This is exactly the case with MMCs, since the number of candidate solutions increases exponentially with the number of possible switch positions. Given that the latter is high due to the big number of used submodules (SMs), it can be understood that use of MPC for MMCs is not an easy task.

Given the above, this paper proposes an MPC algorithm for back-to-back MMCs used in HVDC systems that achieves superior performance by successfully addressing all the relevant control objectives. The MPC problem is simplified by controlling the arm energies based on estimates (instead of measurements) of the SM capacitor voltages. Note that, even though this technique has been shown to be effective with conventional control methods [6], when used in conjunction with MPC lead to increased circulating currents and high current total demand distortion (TDD) as it did not account for the arm energy ripple [7]. Moreover, to tackle the problem of the pronounced computational demands of direct MPC, techniques are implemented in this work that keep the computational complexity of the optimization problem modest. The efficacy of the proposed control scheme is verified with simulations acquired based on MMCs with 20 SMs per arm.

System Modeling

The system under consideration is the back-to-back connected MMCs shown in Fig. 1. Both MMCs consist of three phase legs, each of which is divided into two arms, namely the upper and lower arm. Each arm has N series-connected SMs, and an arm inductor L_{arm}—with internal resistance R_{arm}—to limit fault and circulating currents. The half-bridge SM, as seen in Fig. 1, consists of two pairs of active semiconductor switches with freewheeling diodes and a capacitor C_{SM}, which is ideally maintained at a voltage of v_{dc}/N, where v_{dc} is the dc-link voltage. For the back-to-back HVDC system, resistor R_{loss} is added in parallel to the MMC units to model the switching losses of the converters [2].

The MMC can be controlled by inserting and bypassing SMs into the arms. An inserted SM produces a

voltage of C_{SM} at its terminal, while a bypassed SM has a terminal voltage of zero. Therefore, each of the upper and lower arms can produce $N+1$ different voltage levels. Given this, there are two ways for the MMC to produce the desired output phase voltage, i.e., either by controlling both arms simultaneously such that N SMs are always inserted, or by controlling the SMs of each arm independently from each other. In the former case, the MMC can produce $N+1$ voltage levels at its ac terminals. In the latter, there are $2N+1$ available voltage levels resulting in lower distortion in the output current. Therefore, independent control of the arms is preferable, even though it can lead to a more complicated controller design, or increased computational burden, as in the case of MPC.

Besides the advantages stemming from the independent control of the arms, also controlling each phase independently employs the controller with another degree of freedom, as explained in the following section. Hence, in this section, the single-phase model of the MMC is considered. As the arm voltages depend on the number of inserted SMs, assuming that all capacitors are balanced within an arm, i.e., they all have they same voltage, means that knowledge of which specific SMs are inserted to produce the desired voltage is not required. Therefore, the modeling—and subsequent control—of the MMC can be greatly simplified by considering the number of inserted SMs n_{jx} in each arm $j \in \{u,l\}$ of each phase $x \in \{a,b,c\}$, instead of the switching state of each SM.

Considering the above assumption, the arm voltage v_{jx} produced by the SMs is given by

$$v_{jx} = \frac{n_{jx}}{N} v_{jx}^{\Sigma}, \tag{1}$$

where v_{jx}^{Σ} is the sum of all capacitor voltages in the arm. Assuming that all SMs have the same capacitance C_{SM}, the dynamics of the arm capacitor voltage sums can be described by

$$\frac{\mathrm{d}v_{jx}^{\Sigma}}{\mathrm{d}t} = \frac{n_{jx}}{C_{\mathrm{SM}}} i_{jx}, \tag{2}$$

where i_{jx} is the arm current.

By applying Kirchhoff's current law to the ac terminals, the phase current can be given as

$$i_x = i_{ux} - i_{lx}. \tag{3}$$

Using Kirchhoff's voltage law to the upper and lower arms, the dynamics of the phase legs are governed by

$$L_{\mathrm{g}} \frac{\mathrm{d}i_x}{\mathrm{d}t} + L_{\mathrm{arm}} \frac{\mathrm{d}i_{ux}}{\mathrm{d}t} = \frac{1}{2} v_{\mathrm{dc}} - R_{\mathrm{g}} i_x - R_{\mathrm{arm}} i_{ux} - v_{ux} - v_{\mathrm{g}x}, \tag{4a}$$

$$L_{\mathrm{g}} \frac{\mathrm{d}i_x}{\mathrm{d}t} - L_{\mathrm{arm}} \frac{\mathrm{d}i_{lx}}{\mathrm{d}t} = -\frac{1}{2} v_{\mathrm{dc}} - R_{\mathrm{g}} i_x + R_{\mathrm{arm}} i_{lx} + v_{lx} - v_{\mathrm{g}x}. \tag{4b}$$

Adding (4a) and (4b), and by using (1) and (3), the dynamics of the phase current are described by

$$\left(2L_{\mathrm{g}} + L_{\mathrm{arm}}\right) \frac{\mathrm{d}i_x}{\mathrm{d}t} = \frac{n_{lx} v_{lx}^{\Sigma} - n_{ux} v_{ux}^{\Sigma}}{N} - \left(R_{\mathrm{arm}} + 2R_{\mathrm{g}}\right) i_x - 2v_{\mathrm{g}x}. \tag{5}$$

The upper and lower arm currents consist of a common- and a differential-mode component, i.e.,

$$i_{ux} = i_x/2 + i_{\mathrm{comm},x} \tag{6a}$$

$$i_{lx} = -i_x/2 + i_{\mathrm{comm},x}, \tag{6b}$$

where $i_{\mathrm{comm},x}$ is the common-mode current which flows through both arms and it is defined as

$$i_{\mathrm{comm},x} = \frac{i_{ux} + i_{lx}}{2} = \frac{i_{\mathrm{dc}}}{3} + i_{\mathrm{z}x}, \tag{7}$$

where i_{zx} is the circulating current. As can be observed in (7), in steady-state operation, the common-mode current includes a third of the dc-link current, as the latter is assumed to be equally divided among all phases. In addition, a circulating current component may exist in the common-mode current which is caused by the instantaneous voltage difference between the dc side and the phase leg. Subtracting (4b) from (4a), and with the help of (1) and (7), the common-mode current dynamics are given by

$$2L_{\text{arm}}\frac{\mathrm{d}i_{\text{comm},x}}{\mathrm{d}t} = v_{\text{dc}} - \frac{n_{lx}v_{lx}^{\Sigma} + n_{ux}v_{ux}^{\Sigma}}{N} - 2R_{\text{arm}}i_{\text{comm},x}\,. \tag{8}$$

Following, by inserting (6) into (2), the capacitor voltage sum dynamics can be given as a function of the phase and common-mode currents, i.e.,

$$\frac{\mathrm{d}v_{ux}^{\Sigma}}{\mathrm{d}t} = \frac{n_{ux}}{2C_{\text{SM}}}i_x + \frac{n_{ux}}{C_{\text{SM}}}i_{\text{comm},x}\,, \tag{9a}$$

$$\frac{\mathrm{d}v_{lx}^{\Sigma}}{\mathrm{d}t} = -\frac{n_{lx}}{2C_{\text{SM}}}i_x + \frac{n_{lx}}{C_{\text{SM}}}i_{\text{comm},x}\,. \tag{9b}$$

With the equations derived above that fully describe the dynamics of the MMC, i.e., (5), (8), and (9), the single-phase MMC model can be written in a state-space representation. To this aim, the state vector is chosen as $\boldsymbol{x} = [i_x\ i_{\text{comm},x}\ v_{ux}^{\Sigma}\ v_{lx}^{\Sigma}]^T$, while the input vector is $\boldsymbol{u} = [n_{ux}\ n_{lx}]^T$. As can be seen from the equations the system is nonlinear. Specifically, the model of the MMC is described by the bilinear state-space model as [8]

$$\begin{aligned}\frac{\mathrm{d}\boldsymbol{x}(t)}{\mathrm{d}t} = &\underbrace{\begin{bmatrix} \frac{-R_{\text{arm}}+2R_{\text{g}}}{L_{\text{arm}}+2L_{\text{g}}} & 0 & 0 & 0 \\ 0 & \frac{R_{\text{arm}}}{L_{\text{arm}}} & 0 & 0 \\ 0 & 0 & 0 & 0 \\ 0 & 0 & 0 & 0 \end{bmatrix}}_{\boldsymbol{F}}\boldsymbol{x}(t) + \underbrace{\begin{bmatrix} 0 & 0 & -\frac{1}{N(L_{\text{arm}}+2L_{\text{g}})} & 0 \\ 0 & 0 & -\frac{1}{2NL_{\text{arm}}} & 0 \\ \frac{1}{2C_{\text{SM}}} & \frac{1}{C_{\text{SM}}} & 0 & 0 \\ 0 & 0 & 0 & 0 \end{bmatrix}}_{\boldsymbol{G}_1}u_1(t)\boldsymbol{x}(t) \\ &+ \underbrace{\begin{bmatrix} 0 & 0 & 0 & \frac{1}{N(L_{\text{arm}}+2L_{\text{g}})} \\ 0 & 0 & 0 & -\frac{1}{2NL_{\text{arm}}} \\ 0 & 0 & 0 & 0 \\ -\frac{1}{2C_{\text{SM}}} & \frac{1}{C_{\text{SM}}} & 0 & 0 \end{bmatrix}}_{\boldsymbol{G}_2}u_2(t)\boldsymbol{x}(t) + \underbrace{\begin{bmatrix} -\frac{2v_{\text{g}}(t)}{L_{\text{arm}}+2Lg} \\ \frac{v_{\text{dc}}(t)}{2L_{\text{arm}}} \\ 0 \\ 0 \end{bmatrix}}_{\boldsymbol{g}(t)}\,,\end{aligned} \tag{10}$$

where $\boldsymbol{F}$ is the system matrix, $\boldsymbol{G}_1$ and $\boldsymbol{G}_2$ are the input matrices, $\boldsymbol{g}(t)$ is an offset vector, and u_1 and u_2 are the first and second elements of $\boldsymbol{u}$, respectively.

Finally, for control purposes, the continuous-time state-space model is discretized by using the forward Euler method. This yields

$$\boldsymbol{x}(k+1) = \boldsymbol{A}\boldsymbol{x}(k) + \boldsymbol{B}_1u_1(k)\boldsymbol{x}(k) + \boldsymbol{B}_2u_2(k)\boldsymbol{x}(k) + \boldsymbol{b}(k)\,, \tag{11}$$

with $\boldsymbol{A} = \boldsymbol{I} + \boldsymbol{F}T_s$, $\boldsymbol{B}_1 = \boldsymbol{G}_1T_s$, $\boldsymbol{B}_2 = \boldsymbol{G}_2T_s$ and $\boldsymbol{b} = \boldsymbol{g}T_s$, where T_s is the system sampling interval and $\boldsymbol{I}$ is the identity matrix of the same dimension as $\boldsymbol{F}$.

Control Algorithm

The mathematical model of the MMCs derived in the previous section serves as the prediction model for the proposed MPC-based algorithm. In the sequel of this section, the derivation of the control scheme in question is provided.

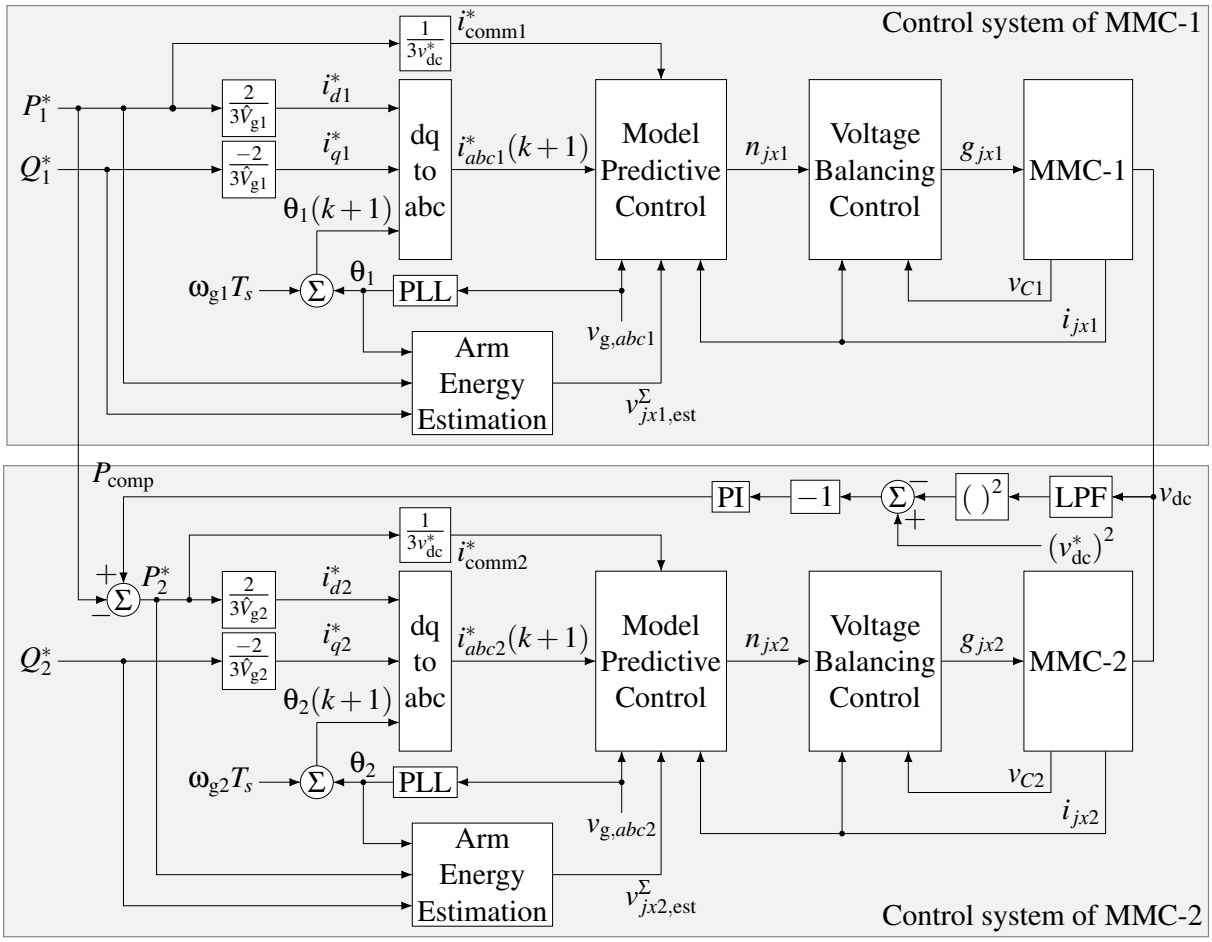

Fig. 2: Complete block diagram of the proposed MPC-based algorithm of the MMC-HVDC system.

Control Structure

The proposed control structure for the MMC-HVDC is shown in Fig. 2. As can be seen, a hierarchical control architecture is adopted which consists of the following three parts:

1. At the upper layer, a PI-based controller controls the dc-link voltage by manipulating the active power reference of MMC-2. In doing so, the controller accounts for the power losses of both MMC units.
2. At the middle layer, as discussed later, the proposed MPC algorithm directly computes the number of the to-be-inserted SMs into each arm to achieve phase current reference tracking and circulating current minimization.
3. At the lower layer, an SM capacitor voltage balancing mechanism selects which individual SMs are inserted/bypassed such that the SM capacitor voltages are balanced. In doing so, the gating signals for the SM switches are generated.

Arm Energy Estimation

Controlling the arm energies, i.e., v^{Σ}_{jx}, can be challenging since the circulating current is used to transfer active power between the converter arms. During steady-state operation the circulating current needs to be minimized. However, during transients, when imbalances in the arm energies occur, a small circulating current is required to redistribute the energy stored in the arms in order to balance them. Typically, this issue is solved by adding an extra component to the common-mode current using PI-based controllers to regulate the total energy and the energy difference between the upper and lower arms [9]. In this paper, however, the open-loop arm energy balancing method proposed in [6] is adopted and utilized in conjunction with MPC.

To this aim, the j arm energy is estimated according to [6]

$$W_{Cj}^{\Sigma} = W_C^{\Sigma *} \pm \frac{\hat{V}_g i_{\text{comm}}^* \cos(\theta)}{\omega_g} \mp \frac{\left(\frac{v_{\text{dc}}^*}{2} - R_{\text{arm}} i_{\text{comm}}^*\right) \hat{I}_x \cos(\theta - \phi)}{2\omega_g} + \frac{\hat{V}_g \hat{I}_x \sin(2\theta - \phi)}{8\omega_g}, \tag{12}$$

where $\hat{V}_g$ and $\hat{I}_x$ are the grid peak voltage and current, respectively, ω_g the grid angular frequency, θ the grid angle, ϕ the power angle, and $W_C^{\Sigma *}$ the average arm energy that is equal to the energy corresponding to the dc-link voltage reference. With (12), the sum of the arm capacitor voltages is given by

$$v_j^{\Sigma} = \sqrt{\frac{2NW_{Cj}^{\Sigma}}{C_{\text{SM}}}}. \tag{13}$$

Using the estimated arm energies works well in steady state and provides a self-stabilizing effect [6]. During transients, when there is an imbalance in the arm energies, a fundamental frequency circulating current appears, which helps to balance the arm energies [10, 11]. This results in a desirable open-loop arm energy balancing, implying that the MPC algorithm does not have to actively address the balancing problem. As a result, the controller design is simplified since the MPC objective function can account only for the grid and circulating currents tracking problem. It is worth mentioning, however, that, as shown in Fig. 2, even though the MPC part of the control structure does not require information about the capacitor voltages, the subsequent voltage balancing controller does. This means that the measurements of the capacitor voltages cannot be completely avoided.

Optimal Control Strategy

Given the open-loop arm balancing startegy described above, the main control objective of the MPC algorithm is to regulate the grid currents along their sinusoidal references so that grid standards, e.g., the IEEE 519 standard [12], are met. Moreover, the circulating currents that may exist in each phase leg need to be minimized to avoid power losses in the phase legs, increase of the switching devices current rating, and pronounced voltage ripples in the SM capacitors [2, 13]. These control tasks need to be met while keeping the average device switching frequency low so that the switching power losses are minimized. Finally, it is noteworthy that the MPC algorithm is not responsible for the SM capacitor voltage balancing, since this task is undertaken by the subsequent balancing controller, as previously mentioned.

With the aforementioned control goals, the objective function for the MPC problem is formulated as

$$J(k) = (\boldsymbol{y}^*(k+1) - \boldsymbol{y}(k+1))^T \boldsymbol{Q} (\boldsymbol{y}^*(k+1) - \boldsymbol{y}(k+1)) + \lambda_u \|\Delta \boldsymbol{u}(k)\|_1, \tag{14}$$

where $\boldsymbol{y} = \begin{bmatrix} i_x & i_{\text{comm},x} \end{bmatrix}^T$ and $\boldsymbol{y}^*$ are the output and corresponding reference vectors, respectively. Moreover, $\Delta \boldsymbol{u}(k) = \boldsymbol{u}(k) - \boldsymbol{u}(k-1)$ indicates the control effort, defined as the difference in the SM modules between two consecutive time steps. Note that $\boldsymbol{Q} = \text{diag}(\lambda_x, \lambda_{\text{comm}})$, with $\lambda_x, \lambda_{\text{comm}} > 0$, and $\lambda_u > 0$ are weighting factors that assign different penalization priorities between the output reference tracking and switching effort terms, respectively. These weighting factors are commonly chosen by examining the Pareto optimal fronts. Finally, it is worth mentioning that function (14) considers the common-mode—rather than the circulating—current since in the single-phase model of the MMC the circulating current cannot be properly predicted due to the coupling of the phases. This, however, does not compromise the controller performance, as the circulating current i_{zx} is effectively eliminated, as shown later.

Considering the big number N of SMs per arm, minimizing (14) in real time for all possible SM combinations can lead to a computationally intractable problem. To keep the computational complexity of the proposed MPC algorithm at bay, the following simplifications are adopted:

1. As already discussed, instead of solving for the optimal switching state of the MMC i.e., switch positions, the direct MPC algorithm computes the optimal number of inserted SMs per arm. This reduces the number of possible solutions from 2^{6N} to $(N+1)^6$.

```
Calculate $i_x$, $i_{\text{comm}}$ and $v_j^{\Sigma}$ with (3), (7) and (13)
$\boldsymbol{x}(k) \leftarrow \begin{bmatrix} i_x & i_{\text{comm}} & v_u^{\Sigma} & v_l^{\Sigma} \end{bmatrix}^T$
$J_{\text{opt}} \leftarrow \infty$
for $\Delta n_u = -\Delta n_{\max}, \ldots, \Delta n_{\max}$ do
    $n_u \leftarrow n_u(k-1) + \Delta n_u$
    if $n_u < 0$ or $n_u > N$ then
        continue
    end if
    for $\Delta n_l = -\Delta n_{\max}, \ldots, \Delta n_{\max}$ do
        $n_l \leftarrow n_l(k-1) + \Delta n_l$
        if $n_l < 0$ or $n_l > N$ then
            continue
        end if
        Calculate $J$ with (14)
        if $J < J_{\text{opt}}$ then
            $J_{\text{opt}} \leftarrow J$
            $n_{u,\text{opt}} \leftarrow n_u$
            $n_{l,\text{opt}} \leftarrow n_l$
        end if
    end for
end for
return $n_{u,\text{opt}}$, $n_{l,\text{opt}}$
```

(a) MPC algorithm.

```
Divide SMs into groups of inserted and bypassed SMs.
Sort the groups by capacitor voltages.
$\Delta n_{jx} \leftarrow n_{jx,\text{opt}}(k) - n_{jx,\text{opt}}(k-1)$
if $\Delta n_{jx} > 0$ then
    if $i_{jx} > 0$ then
        Insert $\Delta n_{jx}$ SMs with the lowest voltages
    else
        Insert $\Delta n_{jx}$ SMs with the highest voltages
    end if
else if $\Delta n_{jx} < 0$ then
    if $i_{jx} > 0$ then
        Bypass $\Delta n_{jx}$ SMs with the highest voltages
    else
        Bypass $\Delta n_{jx}$ SMs with the lowest voltages
    end if
else
    Apply the last-applied gating signals
end if
```

(b) Voltage balancing algorithm.

Fig. 3: Pseudocode of the MPC and voltage balancing algorithms.

2. As mentioned, the direct MPC algorithm controls each phase independently. This reduces the size of the optimization variable from 6 to 2, and, consequently, the possible solutions from $(N+1)^6$ to $(N+1)^2$ per phase.
3. Similar to, e.g., [14], hard constraints $\|\Delta \boldsymbol{u}(k)\|_\infty \leq \Delta n_{\max}$ are added to limit the change in the inserted SMs to $\Delta n_{\max}$ per arm. This limits the possible solutions to $(2\Delta n_{\max}+1)^2$ per phase. As a result, the complexity of the controller is independent of the SM number N, which renders the proposed control scheme feasible for MMCs with any number of SMs. This, however, comes at a cost of a somewhat deteriorated transient performance.

Given the above, the optimization problem underlying direct MPC takes the form

$$\begin{aligned} \underset{\boldsymbol{u}(k)}{\text{minimize}} \quad & J(k) \\ \text{subject to} \quad & \boldsymbol{u}(k) \in \{0, \ldots, N\}^2 \\ & \|\Delta \boldsymbol{u}(k)\|_\infty \leq \Delta n_{\max}, \end{aligned} \tag{15}$$

which is solved by enumerating all possible $(2\Delta n_{\max}+1)^2$ solutions for each phase as shown in the pseudocode of the MPC algorithm provided in Fig. 3a. Finally, it is worth pointing out that the offset vector $\boldsymbol{g}$ in (10) as well as the arm energy estimates (12) depend on the time-varying dc-link voltage. Because the MMC-HVDC system does not have separate dc capacitors, and the independent control of the upper and lower arms gives rise to a time-varying $n_{ux}+n_{lx}$ in the phase legs, the dc-link voltage experiences a high frequency ripple. To avoid the performance deterioration of the MPC-based algorithm, the dc-link voltage reference—instead of its instantaneous value—is used in (10) and (12). Such a simplification, however, can be justified by the fact that an outer-loop is used to regulate the actual dc-link voltage along it reference, meaning that the dc-link voltage is successfully controlled, and its average value is equal to its desired one.

Finally, once the optimal number of SMs per arm is computed, the voltage balancing controller is activated [15]. Note that this controller operates such that not only the SM capacitor balancing is achieved, but also that excessive and unnecessary switching is avoided. In doing so, it is ensured that the device switching frequency remains low. The pseudocode of the balancing algorithm is shown in Fig. 3b.

Table I: HVDC system parameters

Parameter	Symbol	SI Value	Per unit value
Dc-link voltage	V_{dc}	40 kV	1
Rated rms line-to-line voltage	V_{R}	20 kV	0.5
Rated apparent power	S_{R}	30 MVA	1
Grid side resistance	R_{g}	0.05 Ω	0.0015
Grid side inductance	L_{g}	5 mH	0.0481
Arm resistance	R_{arm}	0.1 Ω	0.0031
Arm inductance	L_{arm}	3 mH	0.0289
Submodule capacitance	C_{SM}	6 mF	61.5624
Grid-1 angular frequency	ω_{g1}	$2\pi 50\,\mathrm{rad\,s^{-1}}$	1
Grid-2 angular frequency	ω_{g2}	$2\pi 60\,\mathrm{rad\,s^{-1}}$	1.2
SMs per arm	N	20	

Performance Assessment

To assess the performance of the proposed control scheme under both steady-state and transient operating conditions, simulations are carried out for an MMC-HVDC system with 20 SMs per arm. The system parameters are shown in Table I. The weighting factors are heuristically chosen as $\lambda_x = 1$, $\lambda_{\mathrm{comm}} = 0.35$ and $\lambda_u = 9 \times 10^{-5}$, resulting in an average device switching frequency of 140 Hz. Moreover, the sampling interval is chosen as $T_s = 100\,\mu\mathrm{s}$, while $\Delta n_{\max} = 1$, and the MPC prediction horizon length is $N_p = 1$. All results are shown in the per unit (p.u.) system.

The steady-state performance of the controller is shown in Fig. 4a and Fig. 4b for MMC-1 and MMC-2, respectively. The phase currents accurately track their references, with the associated TDD being as low as 0.8 % for both systems. As a result, the produced harmonics are well below the limits imposed by the IEEE 519 grid standard [12], see the last row in Fig. 4. Furthermore, the circulating currents are effectively eliminated with their rms value being 0.0084 p.u. Finally, the arm energy estimates, shown with dashed lines, are close to the actual arm energies and the arm total capacitor voltage ripple is around 5 % of the nominal value.

To test the transient behavior of the proposed MPC scheme, the active power reference is halved at $t = 40\,\mathrm{ms}$. The corresponding results are shown in Fig. 5a and Fig. 5b for MMC-1 and MMC-2, respectively. Owing to the direct nature of the controller, the phase currents reach their new desired values within only 2 ms. A small spike is observed in the circulating current. Nevertheless, it disappears in less than 2 ms, as the circulating current settles back to zero. Moreover, after the power reference step-change, a low-amplitude fundamental harmonic appears in the circulating currents. This enables the balancing of the capacitor voltages, as verified by the presented results. Finally, the capacitor voltage sums are well balanced even though they are not addressed in the objective function.

To provide further insight into the workings of the proposed MPC algorithm, Fig. 5c shows the active power of MMC-1 for different levels of $\Delta n_{\max}$. Therein, the drawbacks of limiting $\Delta n_{\max}$ can be seen. By limiting $\Delta n_{\max}$ the available voltage to be inserted within a sampling interval is limited, thus causing slower transients. Moreover, as shown in Fig. 5a and Fig. 5b, due to the magnetization of the arm and filter inductors and the small prediction horizon, the settling time is further increased. Larger values of $\Delta n_{\max}$ can achieve faster transients, as shown in Fig. 5c.

Conclusion

This paper proposed a direct MPC scheme to control the grid and circulating currents of back-to-back MMCs. To do so, the number of SMs that need to be inserted is computed by solving a constrained optimization problem in real time. Moreover, an estimation scheme is implemented to provide the arm energies of the MMCs. By using these estimates in the prediction model, open-loop arm energy balancing

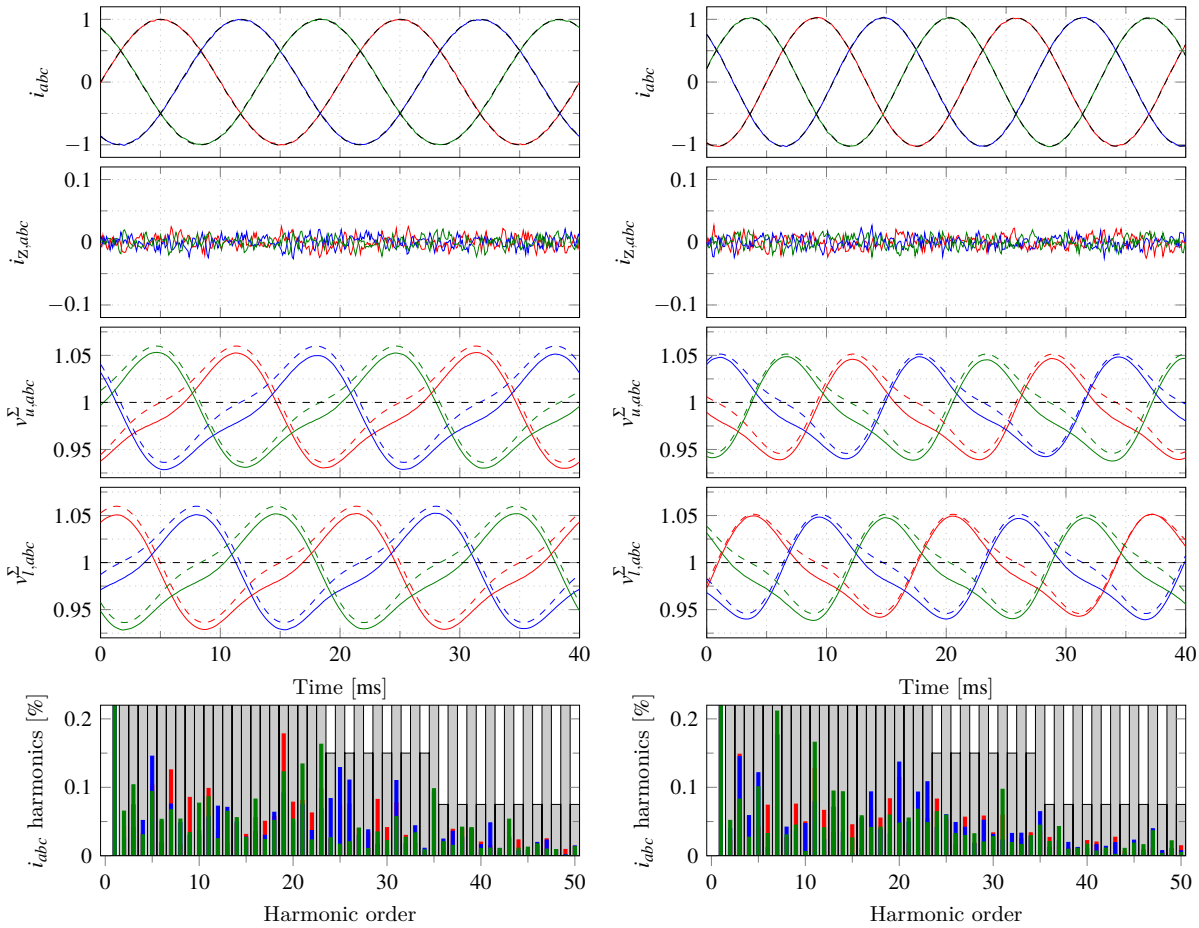

(a) MMC-1 (b) MMC-2

Fig. 4: Steady-state performance for operation under nominal conditions. Top to bottom: grid currents, circulating currents, (measured and estimated) arm total capacitor voltages, grid current harmonic spectra along with the IEEE 519 limits.

is ensured, while potential stability problems are avoided. Consequently, as verified by the presented results, favorable steady-state and transient performance is achieved.

References

[1] A. Lesnicar and R. Marquardt, "An innovative modular multilevel converter topology suitable for a wide power range," in *Proc. IEEE Power Tech. Conf.*, (Bologna, Italy), pp. 1–6, Jun. 2003.

[2] M. Saeedifard and R. Iravani, "Dynamic performance of a modular multilevel back-to-back HVDC system," *IEEE Trans. Power Del.*, vol. 25, pp. 2903–2912, Oct. 2010.

[3] T. Geyer, *Model predictive control of high power converters and industrial drives*. Hoboken, NJ, USA: Wiley, 2016.

[4] P. Karamanakos, E. Liegmann, T. Geyer, and R. Kennel, "Model predictive control of power electronic systems: Methods, results, and challenges," *IEEE Open J. Ind. Appl.*, vol. 1, pp. 95–114, 2020.

[5] P. Karamanakos and T. Geyer, "Guidelines for the design of finite control set model predictive controllers," *IEEE Trans. Power Electron.*, vol. 35, pp. 7434–7450, Jul. 2020.

[6] L. Angquist, A. Antonopoulos, D. Siemaszko, K. Ilves, M. Vasiladiotis, and H.-P. Nee, "Open-loop control of modular multilevel converters using estimation of stored energy," *IEEE Trans. Ind. Appl.*, vol. 47, pp. 2516–2524, Nov./Dec. 2011.

[7] F. Zhang, W. Li, and G. Joós, "A voltage-level-based model predictive control of modular multilevel converter," *IEEE Trans. Ind. Electron.*, vol. 63, pp. 5301–5312, Aug. 2016.

[8] V. Verdult, M. Verhaegen, and V. Verdult, "Bilinear state space systems for nonlinear dynamical modelling," *Theory in Biosc.*, vol. 119, no. 1, pp. 1–9, 2000.

[9] A. Antonopoulos, L. Angquist, and H.-P. Nee, "On dynamics and voltage control of the modular multilevel converter," in *Proc. Eur. Power Electron. Conf.*, (Barcelona, Spain), pp. 1–10, Sep. 2009.

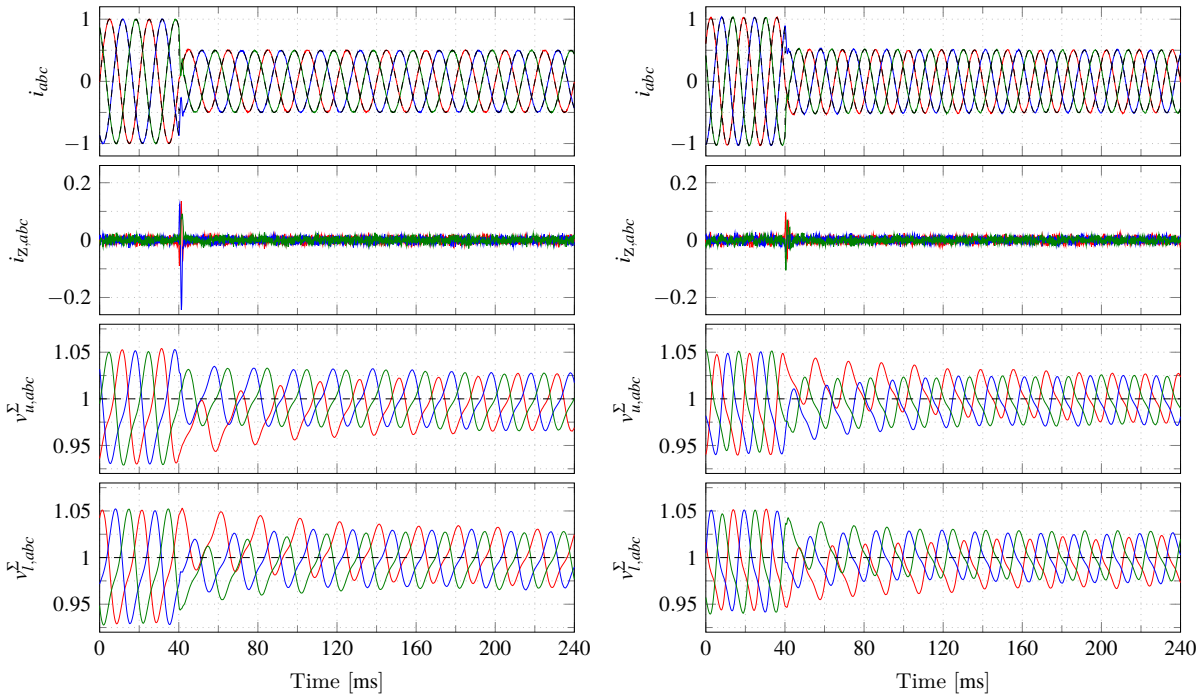

(a) MMC-1 (b) MMC-2

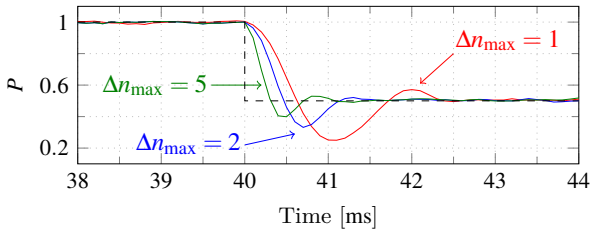

(c) Active power of MMC-1 with varying $\Delta n_{\max}$.

Fig. 5: Transient performance for operation under an active power reference step. Top to bottom: grid currents, circulating currents, measured arm total capacitor voltages.

[10] A. Antonopoulos, L. Ängquist, L. Harnefors, K. Ilves, and H.-P. Nee, "Global asymptotic stability of modular multilevel converters," *IEEE Trans. Ind. Electron.*, vol. 61, pp. 603–612, Feb. 2014.

[11] L. Harnefors, A. Antonopoulos, S. Norrga, L. Angquist, and H.-P. Nee, "Dynamic analysis of modular multilevel converters," *IEEE Trans. Ind. Electron.*, vol. 60, pp. 2526–2537, Jul. 2013.

[12] IEEE Std 519-2014 (Revision of IEEE Std 519-1992), "IEEE recommended practices and requirements for harmonic control in electrical power systems," Jun. 2014.

[13] B. Bahrani, S. Debnath, and M. Saeedifard, "Circulating current suppression of the modular multilevel converter in a double-frequency rotating reference frame," *IEEE Trans. Power Electron.*, vol. 31, pp. 783–792, Jan. 2016.

[14] M. Vatani, B. Bahrani, M. Saeedifard, and M. Hovd, "Indirect finite control set model predictive control of modular multilevel converters," *IEEE Trans. Smart Grid*, vol. 6, pp. 1520–1529, May 2015.

[15] Q. Tu, Z. Xu, and L. Xu, "Reduced switching-frequency modulation and circulating current suppression for modular multilevel converters," *IEEE Trans. Power Del.*, vol. 26, pp. 2009–2017, Jul. 2011.